Journal of Electroceramics, 12, 151–161, 2004

$Pb(Mg_{1/3}Nb_{2/3})O_3$ and $(1-x)Pb(Mg_{1/3}Nb_{2/3})O_3 - xPbTiO_3$ Relaxor Ferroelectric Thick Films: Processing and Electrical Characterization

S. GENTIL, D. DAMJANOVIC & N. SETTER

Ceramics Laboratory, Materials Institute, Faculty of Engineering, Swiss Federal Institute of Technology-EPFL, CH-1015 Lausanne, Switzerland

Submitted March 25, 2002; Revised June 30, 2003; Accepted July 16, 2003

Abstract. The lead magnesium niobate [$Pb(Mg_{1/3}Nb_{2/3})O_3$ or PMN], and its solid solutions with lead titanate ($PbTiO_3$ or PT), are of great interest because of their high electromechanical properties. At large PMN content, these materials exhibit relaxor characteristics with large electrostrictive strains and a large permittivity, while compositions near the morphotropic phase boundary present very interesting piezoelectric properties. So far, properties of these materials in ceramic, thin film and single-crystal form have been investigated. In this paper, we report on preparation and properties of pyrochlore free PMN and 0.65PMN-0.35PT thick films (thickness = 10 to 20 μm). The films were prepared from ethyl cellulose ink by screen printing on alumina substrate. The influence of various parameters, such as powder characteristics, inks formulation and films sintering conditions, on films densification are discussed. The dielectric and electromechanical properties of the films were examined. Relaxor-like behaviour was clearly demonstrated in PMN films. The maximum relative permittivity for PMN film was 10000 (at 0.1 kHz), which is lower than in bulk ceramics (17800 at 0.1 kHz) prepared under the same conditions. For 0.65PMN-0.35PT, the maximum relative permittivity was around 15500 against 24000 in the bulk. Several parameters, which might be responsible for the lower permittivity, are discussed. Poled 0.65PMN-0.35PT thick films exhibit relatively large piezoelectric response (d_{33} up to 200 pm/V) and unipolar strains approaching 0.1%, making these films of interest for various actuator and transducer applications.

Keywords: PMN, PMN-PT, thick films, relaxor, piezoelectric

1. Introduction

The complex perovskite lead magnesium niobate [1] $Pb(Mg_{1/3}Nb_{2/3})O_3$ or PMN, exhibits typical relaxor properties characterized by a diffuse maximum of dielectric constant around -10°C, associated with a strong frequency dispersion. The lead titanate, $PbTiO_3$ or PT, is a typical ferroelectric with ferroelectric to paraelectric phase transition temperature at $T_C = 490^{\circ}$C [2]. Depending on composition, the solid solutions of these materials, $(1-x)$PMN$-x$PT, present a combination of the advantages of both relaxor PMN and ferroelectric PT. At low PT content ($x < 0.1$), $(1-x)$PMN$-x$PT exhibits interesting electrostrictive properties [3, 4], whereas compositions with approximately 30–35% PT exhibit a morphotropic phase boundary (MPB) and large piezoelectric properties [5].

Recently, there has been an increasing interest in miniaturized piezoelectric transducers, for example for high frequency medical imaging applications and microactuators. The screen printing technology is attractive for preparation of miniature ceramic elements because of its simplicity, high yields and low cost. It was successfully applied for preparation of PZT thick films on silicon substrates [6–8]. Despite their attractive piezoelectric properties, only several reports have so far discussed the preparation and properties of lead-based ferroelectric relaxors in thick film form [9, 10].

The purpose of this investigation was to determine the influence of various parameters, such as powder characteristics, inks formulation and sintering process, on densification of screen printed $(1-x)$PMN$-(x)$PT thick films (thickness from 10 to 20 μm) and to investigate their dielectric and electromechanical properties.

The conditions for preparation of pyrochlore free thick films are discussed. Whereas films with compositions ranging from $x = 0$ to $x = 0.40$ were investigated, in this article we report on the preparation and properties of PMN and 0.65PMN-0.35PT films.

2. Experimental Procedure

2.1. Powders Elaboration

Pyrochlore-free PMN and 0.65PMN-0.35PT powders were successfully obtained via a modified columbite route [11], using as starting raw materials powders of PbO, $Mg(CO_3)_4{\cdot}Mg(OH)_2{\cdot}5H_2O$, Nb_2O_5 and TiO_2.

The perovskite and pyrochlore phase formation has been investigated as a function of calcination temperature and time by differential thermal analysis, thermogravimetry (DTA−TG) and X-rays diffraction (XRD). The particles size and their morphology were determined via specific area measurements and scanning electron microscopy (SEM).

In the first step (for PMN or PMN-PT synthesis), columbite, $MgNb_2O_6$ is obtained according to stoichiometric reaction (R.1):

$$Mg(CO_3)_4 \cdot Mg(OH)_2 \cdot 5H_2O + 5Nb_2O_5 \rightarrow 5MgNb_2O_6 \quad \text{(R.1)}$$

The starting powder mixture was ball milled for 48 hours and then calcined. In classical process the columbite was obtained after 4 h at 1150°C (Fig. 1(a)), while in our process we obtained a more reactive and less agglomerated columbite powder (Fig. 1(b)), by calcination at 1000°C for 4 h. The particle size ranged from 0.55 to 1.3 μm with a mean diameter of 0.8 μm.

In the second step, reaction between the columbite and PbO (or PbO and TiO_2) is carried out according to stoichiometric reaction (R.2 or R.3):

$$3PbO + 1MgNb_2O_6 \rightarrow 3PMN \quad \text{(R.2)}$$

$$1PbO + 0.35TiO_2 + 0.65MgNb_2O_6 \rightarrow 1PMN\text{-}PT \quad \text{(R.3)}$$

A mixture of these raw materials was ball milled for 24 h in alcohol. PMN (Fig. 2) and PMN-PT (Fig. 3) powders were obtained by calcination at 800°C for 1 h 45 min in covered alumina crucible. Longer

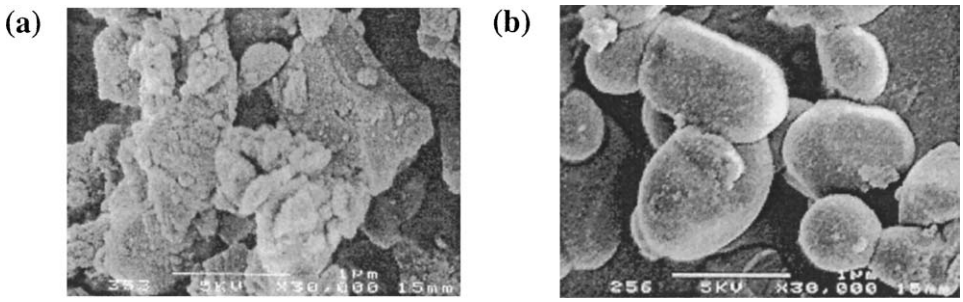

Fig. 1. $MgNb_2O_6$ powders calcined at 1150°C for 4 h (a) and 1000°C for 4 h (b).

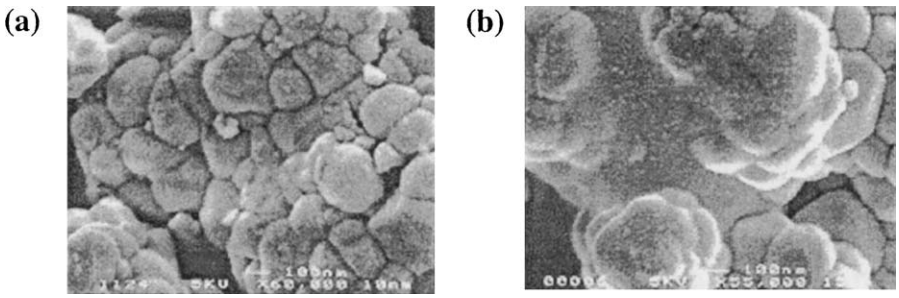

Fig. 2. PMN powders after calcination at 800°C for 1 h 45 min (a) and at 800°C for 3 h (b).

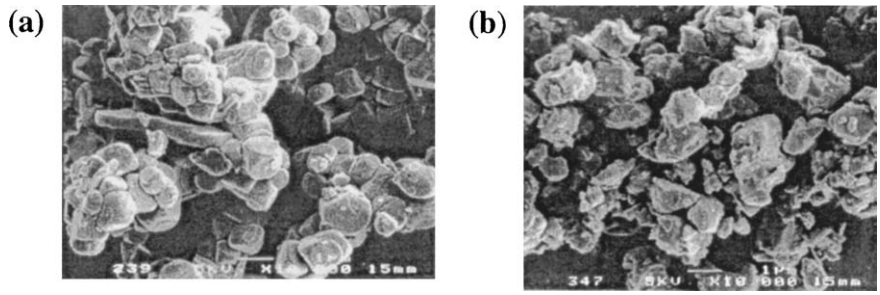

Fig. 3. Effect of ball milling on calcined powder for PMN (a) and $PMN_{0.65}$-$PT_{0.35}$(b).

calcination times lead to coarser powders, as shown in Fig. 2(b).

The calcined powders were crushed and then ground by ball milling for 24 h. After the milling, these powders present particle sizes ranging from 0.35 to 1.3 μm with a mean diameter of 0.6 μm.

The attrition milling for 2 h at 650 rpm breaks the agglomerates and decreases both the maximum and medium size of grains (0.9 μm for the maximum and 0.4 μm for the medium).At each step of powder processing, powder XRD patterns were taken to check the phase purity (Figs. 4 and 5).

The calcined powders were used, without addition of binders, for preparation of ceramics inks and bulk pellets.

2.2. *Thick Films Preparation*

Pyrochlore-free PMN and 0.65PMN-0.35PT thick films were successfully obtained by screen printing. The substrates used for the study were 99.6% alumina substrates (Coors, Superstrate) having the dimensions of $51 \times 51 \times 0.38$ mm^3 and $51 \times 51 \times 0.64$ mm^3, grain size inferior to 1 μm, and 50 nm surface roughness.

The screen printable pastes were prepared by kneading the ground powders with organic vehicles in a three-roll mill during 20 min. Different organic vehicles, consisting of ethylcellulose and α-terpineol, were tested as a function of molecular ethylcellulose weight (Hercules type N: N48, N22 and N7) and as various ethylcellulose content (7, 5 and 3% by volume) and

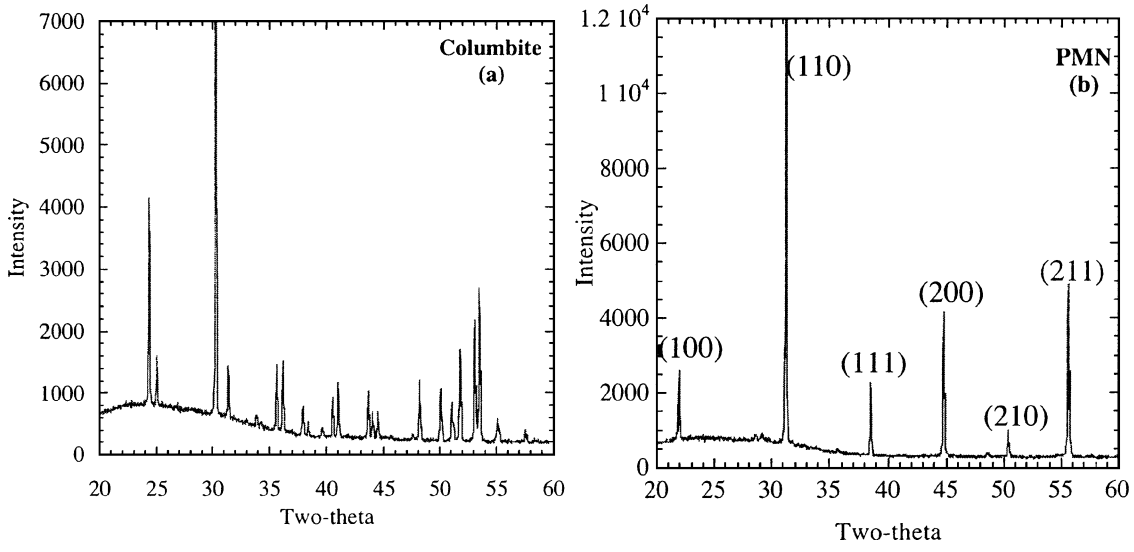

Fig. 4. XRD pattern of intermediate columbite (a) and calcined/milled PMN powders (b).

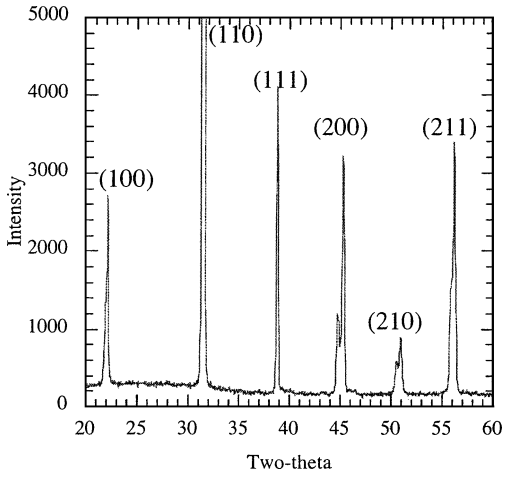

Fig. 5. XRD pattern of calcined and milled 0.65PMN-0.35PT powder.

compared with an industrial formulation from Cerdec (EC3). A dispersing agent PS21A [12] was used to prevent powder agglomeration. Each ink (Pt, PMN and 0.65PMN-0.35PT) is deposited by a DEK screen printer through a 325 mesh stainless steel screen.

The bottom electrodes were produced on alumina substrates by a double print Pt screen printing process [13] with Cerdec Pt ink and then fired at 1300°C for 20 min. The final electrode was 5–6 μm thick with lateral dimensions of 27×27 mm^2. Four ceramics patterns (each in shape of 1×1 cm^2 square) were screen printed onto Pt/Al_2O_3.

After each ceramic deposition, four treatments have to be carried out: (1) to allow the ink levelling it is necessary to wait for half an hour at room temperature, (2) to remove the organic solvents, deposited layer was dried in an oven at 90°C for 30 min, (3) to increase the green density and improve the densification of ceramics layers, a uniaxial pressure of 150 MPa was applied on dried films, and (4) to remove the ethyl cellulose, to obtain a hard layer and to limit the next layer cleaving, the film was heated at 650°C for 1 h. Combinations of these processes permit good bottom electrode coverage, small surface roughness, good cohesion of the different layers and relatively high thick film density.

2.3. Optimisation of Sintering Process

For bulk samples preparation, the ground powder was pressed into disks of 7 mm in diameter and 4.5 mm in thickness at 41 MPa. Analyses in a dilatometer were carried out for different heating rates (range from 3 to 12°C/min) and dwell temperatures (range from 1100 to 1220°C). In all experiments the cooling rate was 20°C/min. These experiments together with subsequent SEM observations were used to determine the best sintering conditions for bulk samples.

The best thick films densification for PMN and 0.65PMN-0.35PT was obtained with a heating rate of 9 to 12°C/min and a sintering temperature between 1094 and 1215°C. The choice of sintering temperature was function of powder composition. For sintering, the bulk samples were placed with the thick film of the same composition in a covered alumina crucible containing P/PZ powder. The samples were sintered from 1 to 180 min over a temperature range from 1094 to 1215°C. The heating rate was 9 to 12°C/min for all experiments. The general mechanisms of densification and grain growth were similar in bulk samples and thick films, but the maximum of densification occurred at lower temperature for the thick films. As an example, a typical top view of a 0.65PMN-0.35PT thick film (sintered at 1184°C for 100 min with a heating rate of 9°C/min) is presented in Fig. 6.

Surfaces of PMN thick films obtained after different heat treatments are presented in Fig. 7. The view (a) in Fig. 7 indicates that some densification occurred already during the heating to the sintering temperature. The (b) and (c) views of Fig. 7 show the influence of the dwell temperature on the grain growth, and the atmosphere influences on the pyrochlore development. The micrograph presented in (d) demonstrates that it is possible to obtain film with a good microstructure at a lower temperature if the heating rate and the dwell time are increased. The similar trends were observed for PMN-PT thick films.

The final thickness of thick film was measured by α-step (200 Tencor KLA). The thickness varied between 10 to 25 μm as a function of layers number. For example, a sintered film thickness of 20 μm requires four successive depositions. After the surface polishing, gold top electrodes (diameter of 650 μm and 520 nm thick) are deposited by sputtering on the samples for the dielectric and piezoelectric measurements.

3. Dielectric and Piezoelectric Properties

To perform the dielectric measurements, an impedance analyser and a chamber with controlled heating and cooling rates were used. The sample temperature

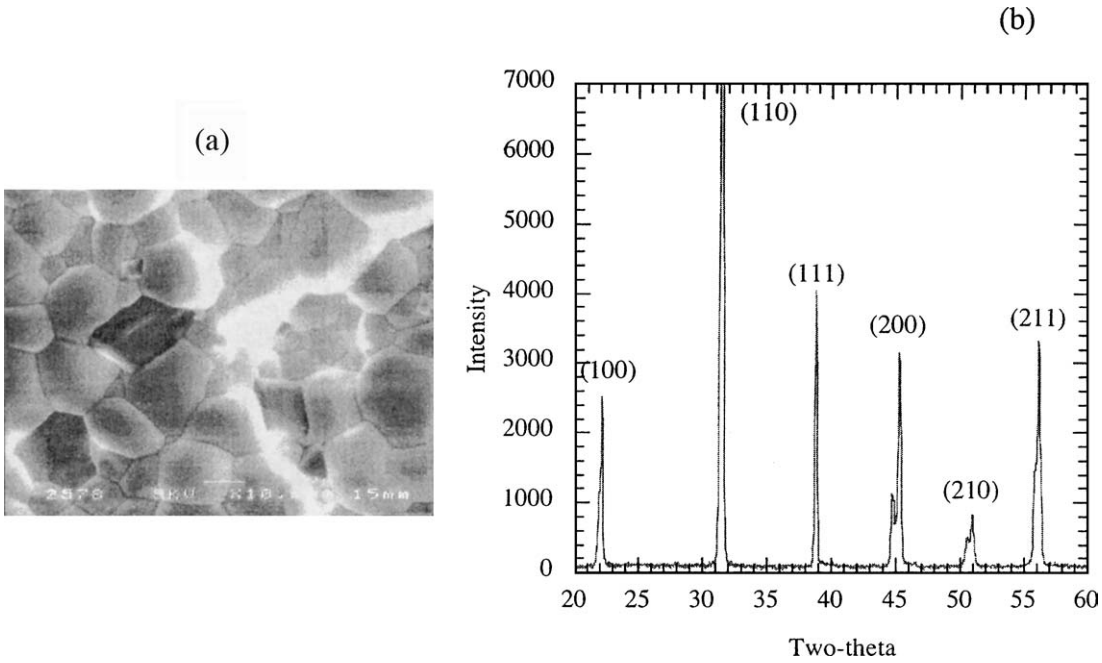

Fig. 6. Plan view SEM of 0.65PMN-0.35PT thick film (a) and corresponding XRD pattern (b).

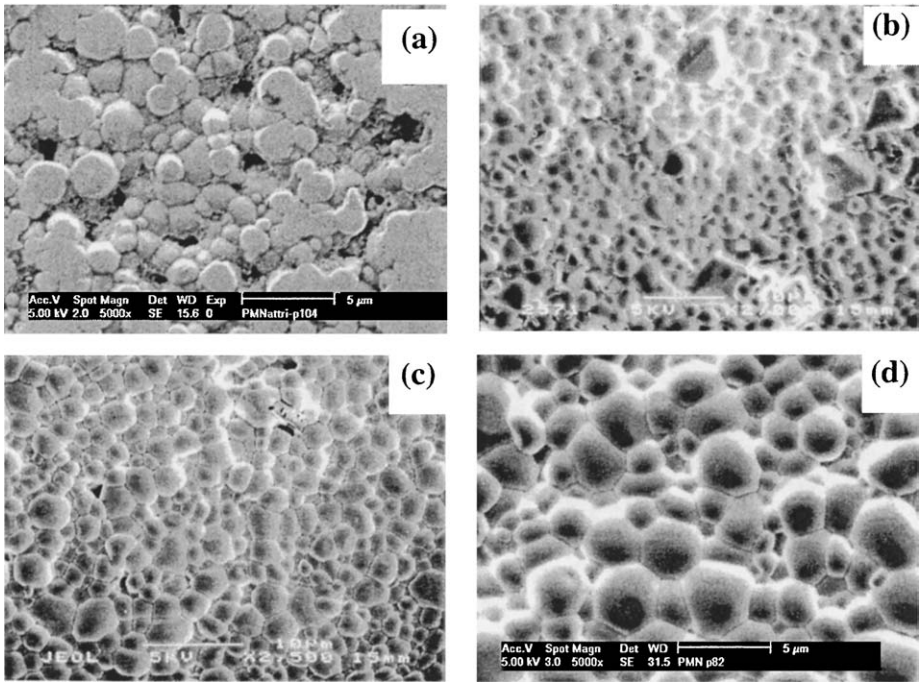

Fig. 7. Plan view SEM of PMN thick films for four different heating treatments and atmospheres. The ink was the same for all samples. (a) 10°C/min - 1215°C/1 min; atmos. P/PZ = 0.84 g; 20 μm thick polished, (b) 9°C/min - 1183°C/100 min; atmos. P/PZ = 0.4 g; 10 μm thick, (c) 10°C/min - 1183°C/120 min; atmos. P/PZ + PMN = 0.64 g; 15 μm thick and (d) 12°C/min - 1163°C/180 min; atmos. P/PZ = 0.62 g; 16 μm thick.

Table 1. Relative permittivity at room temperature as a function of heating treatment for thick films and bulk samples.

PMN	F1	F2	F3	F4	F5	F6
°C/min	9	9	12	10	12	12
Dwell: °C	1183	1184	1094	1215	1163	1163
Time (min)	120	100	180	1	90	180
Thick films	F1	F2	F3	F4	F5	F6
Tickness μm	15	10	12	20	16	15
εr at 1 kHz	7200	6900	6800	7100	6400	5600
Bulk samples	B1	B2	B3	B4	B5	B6
Density g/cm^3	7.72	7.75	7.01	7.37	7.58	7.48
εr at 1 kHz	11900	11900	2000	10600	3300	2300

was measured with a Pt-resistance probe. Polarisation hysteresis loops were obtained by using a charge amplifier and virtual ground condition. A modified Mach-Zehnder laser interferometer was used for the piezoelectric and electrostrictive strain measurements [14].

3.1. Properties of PMN Thick Films

The relative dielectric permittivity at room temperature as a function of different sintering parameters and films thickness is presented in Table 1 for thick films and bulk samples.

For the bulk samples the maximum of densification occurred for the samples sintered at around 1183–1184°C for 100–120 min (F1 and F2 in Table 1). Those samples also exhibited the highest permittivity. With the same heat treatment, good results were also obtained for thick films.

If the sintering temperature was decreased below 1180°C, the bulk samples densification was not optimal and a decrease of relative permittivity was observed even when the sintering time was increased. This was not the case for thick films. A decrease of films' thickness (compare samples F1 and F2) lead to a decrease of dielectric properties. It was also possible to obtain comparable dielectric response for a densification at lower temperature (compare films F3 and F2). In the case of film F4, the good dielectric properties were partly due to an increase in the film thickness and partly due to a higher film density, the latter possible because of the high sintering temperature used despite the short dwell time. While the short firing time reduced the lead losses, it was not sufficient to allow a significant grain growth. For films F5 and F6, an increase of the dwell time improved the densification and increased the grain size. The best dielectric properties are obtained in films with a grain size between 1.5 to 3 μm. The correlation between the grain size and the permittivity was more pronounced in thick films than in bulk samples [15] or in thin films [16].

Figure 8 shows the change of the relative permittivity as a function of temperature at different

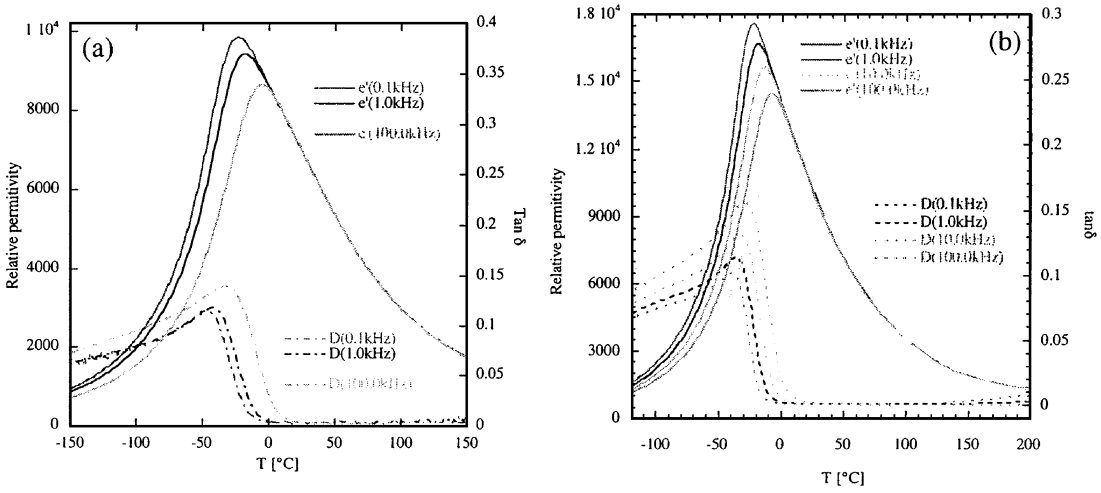

Fig. 8. Temperature and frequency dependence of relative permittivity and dielectric losses in a PMN thick film and a bulk sample. Measurement on thick film were made at 1 kV/cm: (a) PMN thick film (F4); 10°C/min-1215°C/1 min; atmos.P/PZ = 0.84 g, (b) PMN Bulk sample (B2); 9°C/min-1184°C/ 100 min; atmos.P/PZ d = 7.75 (95.4%).

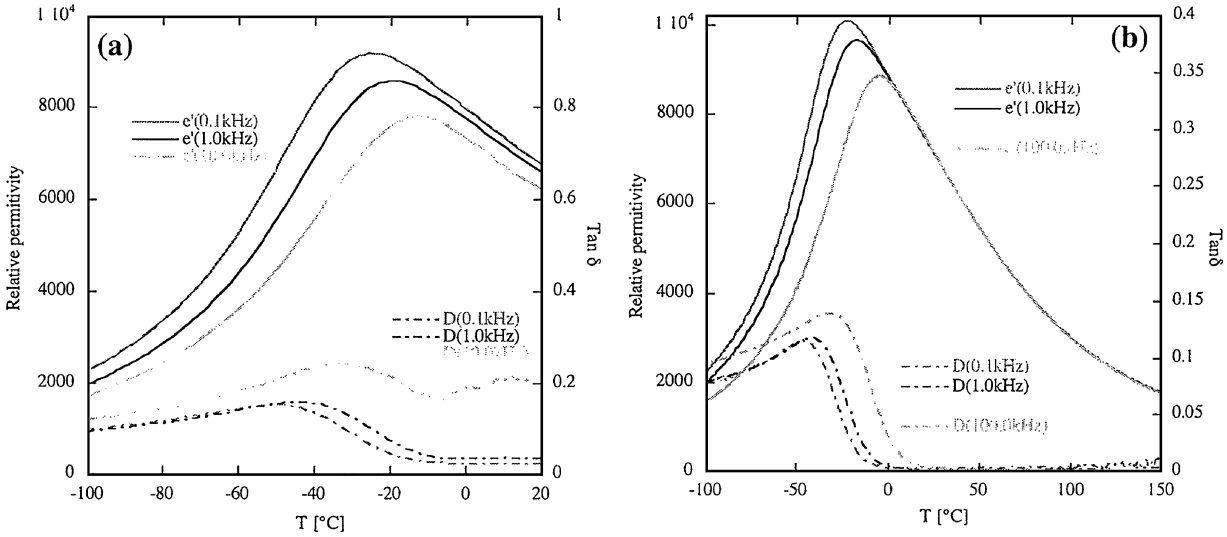

Fig. 9. Influence of the heat treatment and thickness layer on the dielectric response of PMN thick films. Permittivity was measured at 1 kV/cm. Sintering conditions: (a) 9°C/min-1184°C/100', 10 μm thick (film F2) and (b)10°C/min-1212°C/1', 20 μm thick (film F4).

frequencies for the film F4 (Fig. 8(a)) and the bulk sample B2 (Fig. 8(b)).

The relaxor behaviour of the PMN thick film is clearly indicated by the frequency dispersion of the dielectric permittivity maximum. The lower maximum permittivity in PMN thick film (9500 at 1 kHz) with respect to bulk ceramics (16800 at 1 kHz), may result from several effects, including a larger porosity of the films (density $\approx$ 92%), clamping with the substrate, roughness, presence of a second phase or low-dielectric constant layer between the film and bottom electrode that are not detected by XRD measurements and more significant lead evaporation due to a larger surface area of the film (compared to thickness). As shown in Fig. 9 the maximum permittivity at 1 kHz passes from 8600 for a 10 μm thick film to 9700 for a 20 μm thick film.

Since the processing parameters for these films were also different, one cannot, without a more systematic study, correlate this permittivity change exclusively to the thickness variation.

3.2. *Dielectric and Electromechanical Properties of 0.65 PMN-0.35PT Solid Solution*

The most interesting piezoelectric properties in PMN-PT solid solution are expected around the MPB which lies between 30 and 35% PT. In this article we report on the properties of 0.65PMN-0.35PT thick films. The best film, with 96% density was obtained by sintering at 1184°C for 100 min, with a heating rate of 9°C/min. The thickness of this film is 15 μm.

Temperature and frequency dependence of the dielectric permittivity for this MPB composition is shown in Fig. 10. The permittivity exhibits the maximum of 15500 at 1 kHz with $T_C \approx 165$°C compared to

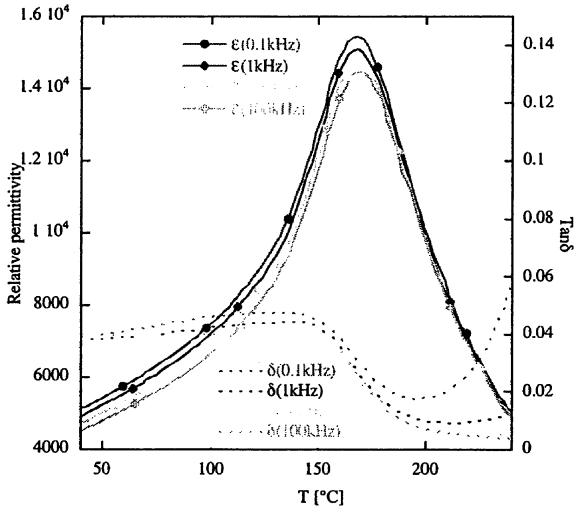

Fig. 10. Temperature and frequency dependence of relative permittivity and dielectric losses in 0.65PMN-0.35PT thick film.

24000 and $T_C \approx 155°C$ in the bulk sample of the same composition. This maximum in the permittivity indicates the paraelectric-ferroelectric phase transition. In contrast to the typical relaxor behaviour in pure PMN or in $(1-x)$PMN-xPT (with $x \leq 0.1$), in 0.65PMN-0.35PT thick film the maximum of permittivity at various frequencies occurs nearly at the same temperature, T_C.

The transition temperature T_C in the film is higher than in the bulk ceramics. This could be due to a presence of stresses in the film, as observed in simple perovskites [17] or associated to a Ti^{4+} gradient [18]. As it is shown in Fig. 11 the film exhibits some preferential orientation with respect to bulk ceramic samples. In ceramics the (00ℓ) peaks have the higher intensity than $(\ell 00)$ peaks, while the opposite is observed in the films.

The polarisation loops for this film at different ac fields are shown in Fig. 12. At room temperature the remanent polarization P_r and a coercive field E_C were respectively 15.6 μC/cm^2 and 6.67 kV/cm for an applied field of 20 kV/cm. If the polarisation loops are measured on a virgin film, an increase in the P_R and decrease in the E_C are observed with increasing number of cycles, as shown in Fig. 12(b). The change in P_R (increase) and E_C (decrease) probably indicates that the domain walls are pinned in the virgin film and get free from the pinning centres by application of the switching field [19].

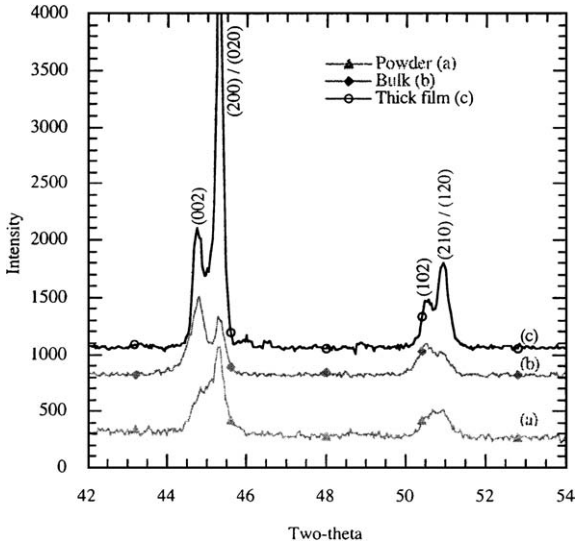

Fig. 11. Difference of orientation between thick film and bulk, comparison with powder X-rays pattern.

The longitudinal d_{33} piezoelectric coefficient as a function of dc electric field is shown in Fig. 13. The shape of the piezoelectric loop is similar to those reported in thin films of $Pb(Zr,Ti)O_3$(PZT). The value of remanent d_{33} is about 180 pm/V, much larger than for typical sputtered PZT films [20] but smaller than expected (600–700 pm/V) for ceramics of the similar composition [21]. The reasons for the lower piezoelectric response in the films is presently being investigated and could probably be related to the clamping of the film by the substrate and the low permittivity of the films [18].

After poling the film at 26 kV/cm for several minutes at room temperature the dependence of the d_{33} and the relative permittivity $\varepsilon_{33}/\varepsilon_0$ on the driving field amplitude was measured at 5 kHz. The results are shown in Fig. 14.

Both coefficients exhibit nonlinearity, which is similar for the permittivity and the piezoelectric coefficient (12–15% increase in the range of fields examined). The linear dependence of the permittivity and the piezoelectric coefficient on the field amplitude indicate domain wall contribution to the polarization and piezoelectric strain, as observed in bulk materials [18, 22]. Similar degree of the nonlinearity for the two coefficients suggests that the probable source of the nonlinearity is displacement of non-180° domain walls, which contribute to both polarization and strain, whereas 180° walls are either relatively immobile or removed during the poling [23]. Maximum measured d_{33} is >200 pm/V. This value is comparable to that in hard PZT ceramics [24].

The aging of the dielectric and piezoelectric responses was measured under weak field conditions (5 kHz, 0.07 kV/cm) after the dc field (26 kV/cm) was held for 1 min and then removed. Both d_{33} and relative permittivity decreased with the time as shown in Fig. 15. After 1 h, d_{33} decreases by about 6% and relative permittivity by 2%, which is less than in PZT thin films and comparable to what is reported for bulk PZT ceramics [25].

Finally, as shown in Fig. 16, the measurements of unipolar strain ($E_{dc} = 16$ kV/cm, $E_{ac} = 33$ kV/cm peak-to-peak) show relatively large total strain in the 0.65PMN-0.35PT film, approaching 0.1% at $E_{dc} + E_{ac} > 35$ kV/cm. This value is close to that in PZT ceramics [26] and is interesting for micro-actuator applications.

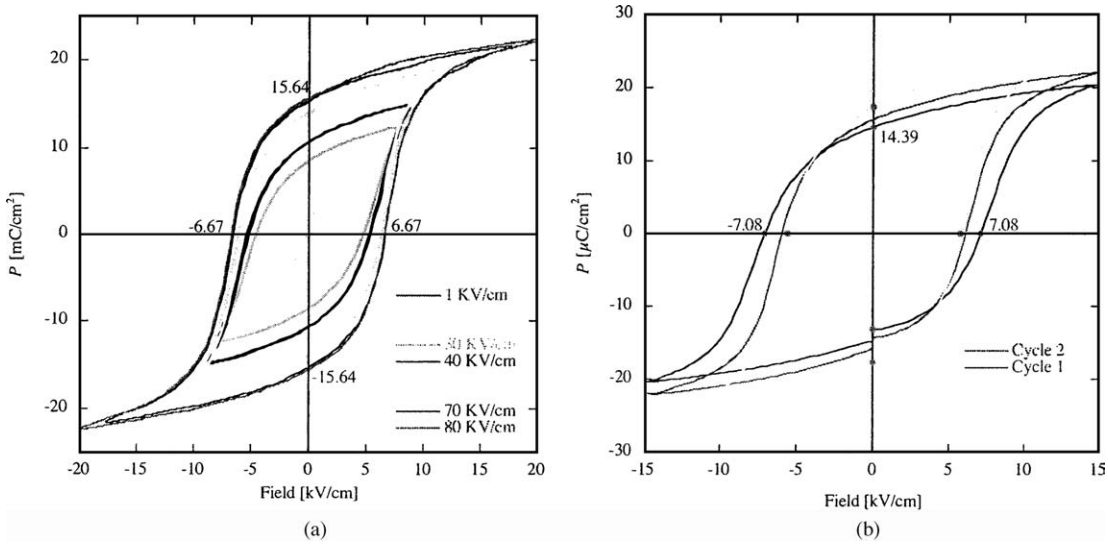

Fig. 12. Polarisation-field hysteresis loop at room temperature, for 15 μm thick 0.65PMN-0.35PT film fired at 1184°C for 100 min (result obtained on two different electrodes on the same film). (a) Polarization as a function of applied ac field and (b) hysteresis loop evolution as a function of number of cycles.

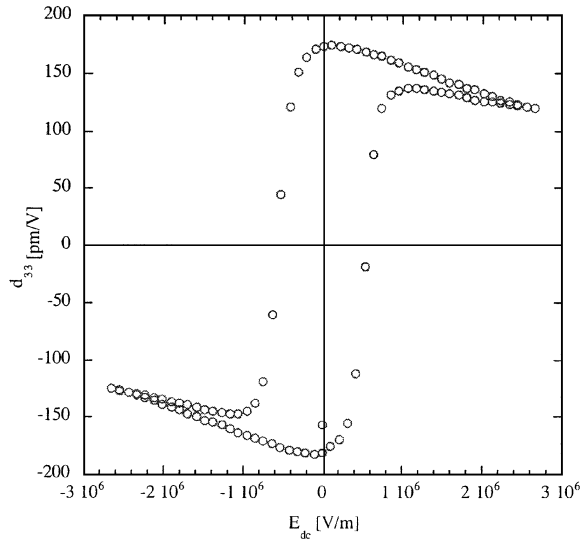

Fig. 13. The longitudinal d_{33} piezoelectric coefficient as a function of dc electric field of the 15 μm thick 0.65-0.35PT film. The d_{33} coefficient was measured by applying an ac field of 0.07 kV/cm at 5 kHz.

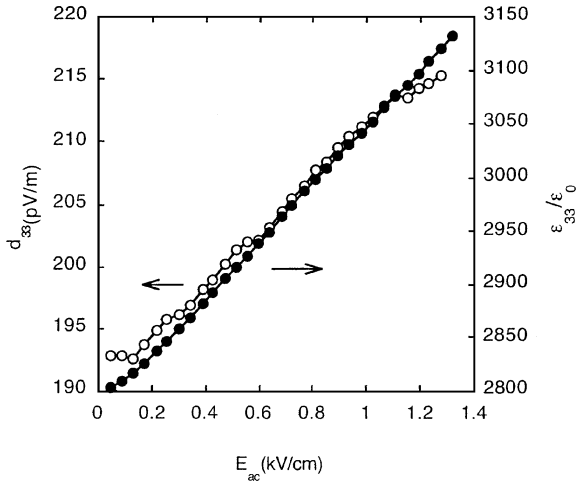

Fig. 14. The longitudinal piezoelectric coefficient d_{33} (open circles) and relative permittivity $\varepsilon_{33}/\varepsilon_0$ (closed circles) as a function of the driving field amplitude E_{ac}.

4. Summary

Pyrochlore free relaxor PMN and relaxor-ferroelectric 0.65PMN-0.35PT thick films are successfully obtained by screen-printing on alumina substrate with screen printed Pt bottom electrode. The sintering conditions used to achieve dense thick films are defined for calcined powders with a medium grain size of 0.4 μm.

The dielectric measurements on PMN and 0.65PMN-0.35PT thick films (fired at 1184°C for 100 min) showed a lower dielectric constant (respectively 9700 and 15500) than in bulk samples. However, our results indicate that these properties can be

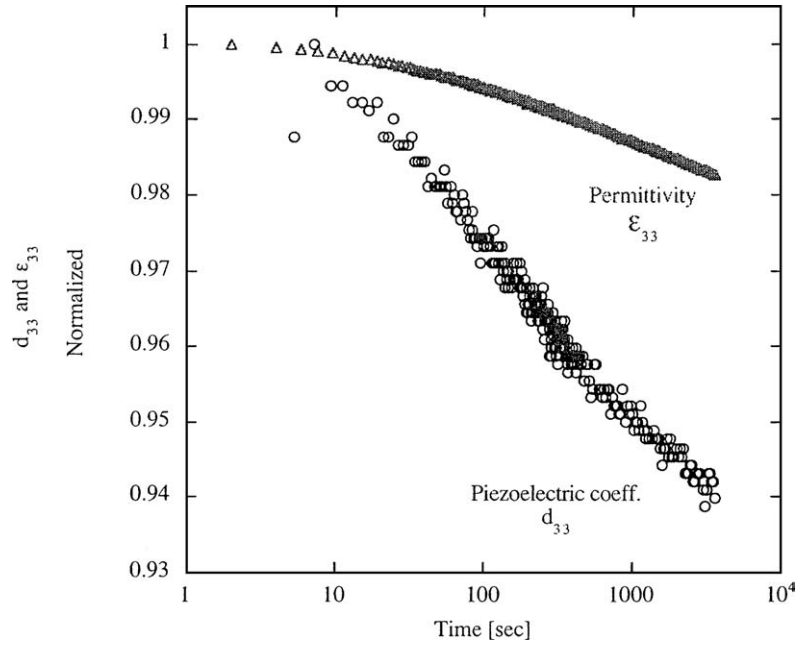

Fig. 15. Aging of the permittivity ε_{33} and the d_{33} piezoelectric coefficient for 15 μm 0.65PMN-0.35 thick film.

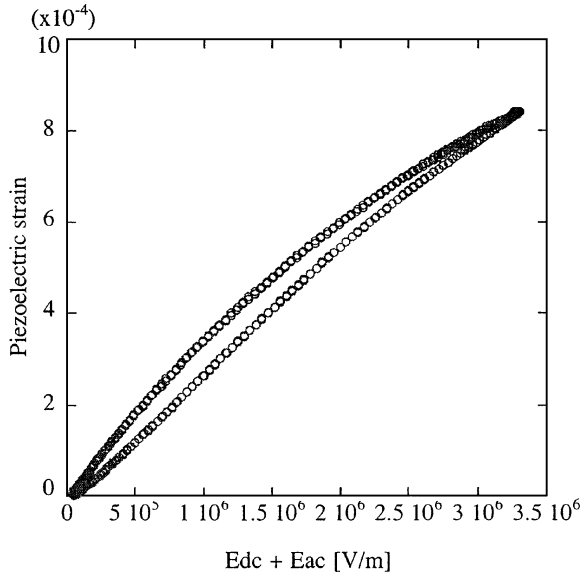

Fig. 16. Unipolar piezoelectric strain vs amplitude of ac electric field amplitude. The measurements were made at 431 Hz under 25 V dc field and 50 V peak-to-peak amplitude of the ac field.

improved by increasing the film thickness and the grain size.

A remanent polarisation of 15.6 μC/cm^2 and a small coercive field of 6.67 kV/cm were obtained for a 15 μm thick 0.65PMN-0.35PT film. The longitudinal piezoelectric coefficient of 200 pm/V and unipolar strain of over 0.08% were measured on the same film.

Acknowledgment

The authors would like to thank J. Mueller for helpful discussions on thick film processing and to J. Castano for his help in powder preparation. The electron microscopy work was performed at the CIME (EPFL). This work was supported by the Swiss OFES in the framework of the European FP5 project PIRAMID.

References

1. G.A. Smolenskii and A.I. Agranovuskaya, *Sov. Phys. Tech. Phys.*, **3**, 1380 (1958).
2. M.E. Lines and A.M. Glasss, *Principles and Applications of Ferroelectrics and Related Materials*, Clarendon Press Oxford, (1977).
3. T.C. Reiley, J.V. Badding, D.A. Payne, and D.A. Chance, *Mater. Res. Bull.*, **19**, 1543 (1984).
4. T. Yamamoto, N. Iwase, M. Harata, and M. Segawa, *Int. J. Hydbrid Microelectron*, **12**, 156 (1989).
5. O. Noblanc, P. Gaucher, and G. Calvarin. *J. Appl. Phys.*, **79**(8), 4291 (1996).

6. R. Mass, M. Koch, N.R. Harris, N.M. White, and A.G.R. Evans, *Materials letters*., **31**, 109 (1997).
7. H.D. Chen, K.R. Udayakumar, L.E. Cross, J.J. Bernstein, and L.C. Niles, *J. Appl. Phys*., **77**(7), 3349 (1995).
8. Y. Akiyama, K. Yamanaka, E. Fujisawa, and Y. Kowata, *Jpn. J. Appl. Phys*., **38**, 5524 (1999).
9. T. Futakuchi, Y. Matsui, and M. Adachi, *Jpn. J. Appl. Phys*., **38**, 5528 (1999).
10. T. Futakuchi and K. Tanino, *Jpn. J. Appl. Phys*., **34**, 5207 (1995).
11. S.J. Butcher and M. Daglish, *Third Euro-Ceramics Conference Proceedings*, **2**, 121 (1993).
12. E.S. Thiele and N. Setter, *J. Am. Cera. Society*., **83**(6), 1407 (2000).
13. J.B. Vechembre and G.R. Fox, *J. Mater. Res*., **16**, 922 (2001).
14. A.L. Kholkin, C. Wütchrich, D. V. Taylor, and N. Setter, *Rev. Sci. Instrum*., **67**, 1935 (1996).
15. P. Papet, J.P. Dougherty, and T.R. Shrout, *J. Mater. Res*., **5**, 2902 (1990).
16. Z. Kighelman, D. Damjanovic, and N. Setter, *J. Appl. Phys*., **82**(2),1393 (2001).
17. V.G. Koukhar, N.A. Pertsev, and R. Waser, *Phys. Rev*., **B 64**, 214103 (2001).
18. A.D. Hilton, D.J. Barber, C.A. Randall, and T.R. Shrout, *J. Mater. Sci*., **25**, 3461 (1990).
19. D. Damjanovic, *Rep. Prog. Phys*., **61**, 1267 (1998).
20. S. Hiboux, P. Muralt, and T. Maeder, *J. Mat. Res*., **14**, 4307 (1999).
21. E. M. Sabolsky, A.R. James, S. Kwon, S. Trolier-McKinstry, and G.L. Messing, *Appl. Phys. Lett*., **78**, 2553 (2001).
22. D. Damjanovic, *J. Appl. Phys*., **82**, 1788 (1997).
23. L.E. Cross, in *Ferroelectric Ceramics*, edited by N. Setter and E.L. Colla (Birkhäuser, Basel, 1993), pp. 1–86.
24. B. Jaffe, W.R. Cook, and H. Jaffe, *Piezoelectric Ceramics* (Academic, New York, 1971).
25. A.L. Kholkin, A.K. Tagantsev, E.C. Colla, D.V. Taylor, and N. Setter, *Integrated Ferroelectrics*, **15**, 317 (1997).
26. S.E. Park and T.R. Shrout, *J. Appl. Phys*., **82**, 1804 (1997).